Analytica Chimica Acta 1232 (2022) 340449

Contents lists available at ScienceDirect

Analytica Chimica Acta

journal homepage: www.elsevier.com/locate/aca

A novel fluorescence biosensor based on double-stranded DNA branch migration-induced HCR and DNAzyme feedback circuit for sensitive detection of *Pseudomonas aeruginosa* (clean version)

Yaxing Xie [a], Guoming Xie [b], Jinshan Yuan [a], Jianhong Zhang [a], Yujun Yang [b], Yuan Yao [c], You Wu [b], Dan Bai [b], Kena Chen [b], Baiying Li [b], Lin Song [b], Hui Chen [a,*]

[a] *Clinical Laboratories, The First Affiliated Hospital of Chongqing Medical University, Chongqing, 400016, PR China*
[b] *Key Laboratory of Laboratory Medical Diagnostics, Chinese Ministry of Education, Department of Laboratory Medicine, Chongqing Medical University, Chongqing, 400016, PR China*
[c] *The Center for Clinical Molecular Medical Detection, The First Affiliated Hospital of Chongqing Medical University, Chongqing, 400016, PR China*

HIGHLIGHTS

- Double-stranded DNA branch migration was firstly applied to bacterial biosensing.
- Both HCR and DNAzyme feedback circuit were contributed to amplify the signal.
- Protein enzymes and complex signal amplification procedures are not required.
- The biosensor exhibits high sensitivity and specificity for detecting *P. aeruginosa*.

GRAPHICAL ABSTRACT

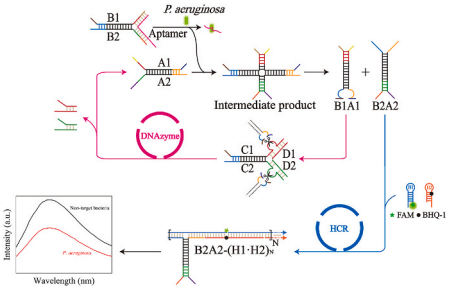

ARTICLE INFO

Keywords:
DNA branch migration
Hybridization chain reaction
DNAzyme
Fluorescence biosensor
Pseudomonas aeruginosa

ABSTRACT

Pseudomonas aeruginosa (*P. aeruginosa*) is one of the most common bacteria in nosocomial infection. Here, a novel fluorescence biosensor based on double-stranded DNA branch migration-induced hybridization chain reaction (HCR) and DNAzyme feedback circuit was constructed for sensitive detection of *P. aeruginosa*. The binding of *P. aeruginosa* with its aptamer on a DNA three-way junction structure initiated the double-stranded DNA branch migration to form two DNA "Y" junction structures. One DNA "Y" junction structure opened the fluorescence-labelled DNA hairpins and triggered the HCR. The other DNA "Y" junction structure formed a double-stranded DNAzyme and cleaved the specific ribonucleotide site, producing new triggering probes to start the next cycle of the double-stranded DNA branch migration. Ultimately, a large number of DNA "Y" junction structures were produced, which greatly promoted signal amplification. Under optimized conditions, the proposed biosensor detected a wide linearity range of 10^2–10^7 CFU mL^{-1}, and the limit of detection was 37 CFU mL^{-1} (S/N = 3). The recovery test results indicated that the biosensor has promising clinical application potential. Because of the simultaneous initiation of the HCR and the DNAzyme feedback circuit through the double-

* Corresponding author. Clinical Laboratories, The First Affiliated Hospital of Chongqing Medical University, No. 1, You Yi Road, Yu-zhong District, Chongqing, 400016, PR China.
E-mail address: huichen@cqmu.edu.cn (H. Chen).

https://doi.org/10.1016/j.aca.2022.340449
Received 27 July 2022; Received in revised form 18 September 2022; Accepted 25 September 2022
Available online 28 September 2022

stranded DNA branch migration, the constructed biosensor provided an ideal platform for pathogenic bacteria detection without protein enzymes and complex signal amplification procedures.

1. Introduction

Bacterial infection has become a major threat to public health worldwide, and it can cause serious consequences for people's health and wellbeing [1]. Among the various pathogenic bacteria, *Pseudomonas aeruginosa* (*P. aeruginosa*) is one of the most common bacteria in nosocomial infections [2]. Its infections are associated with high morbidity and mortality in hospitalized patients with compromised immune systems [3]. At present, conventional detection methods for *P. aeruginosa* include plate culture, polymerase chain reaction (PCR) and mass spectrometry. As the gold standard, plate culture is accurate but labor-intensive and time-consuming [4]. PCR is commonly used for clinical diagnoses, but it requires strict protocols and professionally trained operators [5]. Mass spectrometry also requires large-scale and sophisticated instruments [6]. Consequently, it is essential to develop a both sensitive and rapid method for the detection of *P. aeruginosa.*

To this end, biosensors have been explored for the detection of pathogenic bacteria and include electrochemiluminescence biosensors [7], colorimetric biosensors [8], fluorescence biosensors [9], and nanomachine biosensors [10]. Among these methods, fluorescence biosensors have attracted considerable attention due to their ease of operation, high speed and capacity for high-throughput screening [11]. Utilizing the specific binding of biological recognition molecules (for example, nucleic acids, and enzymes) and target analyte, the fluorescence biosensors can realize the specific biological recognition sensing [12]. Furthermore, the development of DNA nanotechnology and materials promoted the multifunctional and generalized applications of fluorescence biosensors. For example, Qiu et al. developed an all-in-one paper-based analytical device for visual and sensitive fluorescence detection of carcinoembryonic antigen by combining quantum dot-enzyme-impregnated paper with DNA-gated mesoporous silica nanocontainers [13]. The bacterial concentration is often extremely low in the early stage of infection. Therefore, many signal amplification methods have been developed in combination with fluorescence biosensors, such as rolling circle amplification (RCA) [14], strand displacement amplification (SDA) [15], catalytic hairpin assembly (CHA) [16], and hybridization chain reaction (HCR) [17]. Recently, HCR has attracted much attention due to its simple operating procedure, gentle reaction condition and high versatility [18]. In the presence of triggering chains, long dsDNA polymers can be generated due to a self-sustained hybridization reaction of two metastable DNA hairpins [19]. Unlike other signal amplification methods, HCR is a characteristic isothermal signal amplification strategy and does not require protein enzymes [20]. Thus, HCR can be utilized as a signal amplification method to construct fluorescence biosensors for bacterial detection. However, a single HCR has a relatively low reaction velocity and amplification efficiency, which limits its application for analysing trace amounts of biomarkers [21]. Owing to these circumstances, many improved strategies have been proposed. For example, Yang et al. reported a branched HCR signal amplification method for the detection of Pb^{2+} [22]. A nonlinear HCR has also been reported for detecting miRNA [19]. These methods overcome some defects of conventional HCR, but they are still faced with the problem of low efficiency or complex procedures [23].

DNAzymes are a type of DNA molecule with a variety of specific catalytic functions [24,25]. Compared with protein enzymes, DNAzymes have some natural advantages, such as good stability, easy synthesis and modification, and low preparation costs [26,27]. Therefore, DNAzymes are often applied in combination with other signal amplification methods. DNAzyme feedback circuit is a cyclic system for signal amplification [28]. In this system, more products are accumulated via a new cleaving cycle [29]. Recently, Wei et al. reported a HCR driving DNAzyme feedback circuit for in vitro and in vivo amplified miR-21 imaging [21]. By integrating HCR and a DNAzyme, the method achieved a lower detection limit compared with HCR alone. Therefore, in the present work, the combination of HCR with a DNAzyme feedback circuit was considered to be an ideal method for detecting pathogenic bacteria.

Double-stranded DNA branch migration, also known as Holliday junction, is a nucleic acid hybridization method commonly used for the detection of single nucleotide polymorphisms (SNPs) because of its specific double recognition of SNP sites [30–32]. However, this method has not been reported in the field of non-nucleic acid target detection. Notably, by undergoing a series of four-stranded states, two DNA "Y" junction structures are produced eventually via the double-stranded DNA branch migration. The two DNA "Y" junction structures are ideal initiators that simultaneously trigger the HCR and the DNAzyme feedback circuit because of the linked branches at their ends [33]. Furthermore, the protruding branches can bind with *P. aeruginosa* aptamer through Watson-Crick base pairing. Aptamers are DNA or RNA sequences that can identify a variety of target molecules with high specificity and affinity [34]. In our team's previous work, the aptamer was used as a recognition element for the detection of *Escherichia coli* [35] and staphylococcal enterotoxin B [36]. Herein, inspired by the above strategies, a novel fluorescence biosensor was constructed for the detection of *P. aeruginosa*. The aptamer was used to ensure recognition specificity. In the presence of *P. aeruginosa*, two DNA "Y" junction structures were produced through the double-stranded DNA branch migration. The HCR and the DNAzyme feedback circuit were triggered simultaneously by the DNA "Y" junction structures, which greatly promotes the signal amplification capacity. Signal amplification induced by the double-stranded DNA branch migration does not require protein enzymes and complex signal amplification procedures, which provides an ideal fluorescent detection platform for pathogenic bacteria. The biosensor had good sensitivity and specificity, which also showed great clinical application potential.

2. Material and methods

2.1. Reagents and apparatus

P. aeruginosa (ATCC 27853) was obtained from the American Type Culture Collection (ATCC, USA). *Staphylococcus aureus* (*S. aureus*), *Escherichia coli* (*E. coli*), *Acinetobacter baumannii* (*A. baumannii*) and *group B streptococcus* (GBS) were obtained from the First Affiliated Hospital of Chongqing Medical University. Tris(hydroxymethyl)-aminomethane hydrochloride (Tris-HCl, 1 M, pH 7.8), 4-(2-hydroxyethyl) piperazine-1-ethanesulfonic acid (HEPES, 1 M, pH 7.8), phosphate buffered saline (PBS, pH 7.4), sodium chloride and magnesium chloride were obtained from Sangon Biotechnology, Co. (Shanghai, China). All materials and reagents used in this work were used directly without any purification. DNA oligonucleotides were synthesized and purified by high-performance liquid chromatography at Beijing Genomics Institute (BGI). DNA hairpins were heated to 95 °C for 3 min and then cooled to room temperature (25 °C) for 2 h before use. Ultrapure water (Milli-Q 18.2 MΩ cm, Millipore, Inc) was employed in all of the experiments. The sequences of all oligonucleotides are listed in Table S1. The reference aptamer sequence was previously identified with SELEX method [37].

The recognition effect between the aptamer and *P. aeruginosa* was analysed by upright fluorescence microscopy (Nikon ECLIPSE 80i, Japan). Fluorescence measurements were carried out on a Cary Eclipse

fluorescence spectrophotometer (Agilent Technologies, USA). A T100™ Thermal Cycler (Bio-Rad, USA) was used to heat the DNA hairpins. The gel electrophoresis images were obtained using an electrophoresis apparatus (DYY-6C, LIUYI, China) and imaging system (Bio-Rad Laboratories, USA).

2.2. Bacterial culture

LB broth medium (500 mL) was prepared with 5 g sodium chloride, 5 g tryptone, 2.5 g yeast extract, 7.5 g agarose and 500 mL of ddH_2O. *P. aeruginosa* and the other bacterial strains were cultured on LB plates in an incubator containing 5% CO_2 at 37 °C for 16–24 h. Fresh bacteria in PBS were obtained by washing the plates with sterile PBS, and the number of bacteria was determined by McFarland turbidimetry. Bacterial suspensions of different concentrations (10^2, 10^3, 10^4, 10^5, 10^6, 10^7 and 10^8 CFU mL^{-1}) were prepared in PBS.

2.3. Specific binding ability between the aptamer and P. aeruginosa

A FAM-labelled aptamer was chosen to verify the specific binding activity between the aptamer and *P. aeruginosa*. *P. aeruginosa*, *S. aureus* and *A. baumannii* (the latter two were negative controls) were incubated in a 200 nM fluorescent *P. aeruginosa* aptamer solution for 2.5 h at room temperature, respectively. Afterwards, the solution was centrifugated at 5000 rpm for 5 min, then the sediment and supernatant were collected, respectively. The sediment samples were observed by fluorescence microscopy and the supernatant was measured by Cary Eclipse fluorescence spectrophotometer (excitation and emission wavelengths: 490 nm and 520 nm, respectively; excitation and emission slits: 5 nm each).

2.4. Polyacrylamide gel electrophoresis

Polyacrylamide gel electrophoresis (PAGE) was performed to verify the feasibility of the double-stranded DNA branch migration and HCR,. In brief, the samples were injected into a 12% native polyacrylamide gel and electrophoresis was performed at 130 V for 50 min. The gel was then stained with 4S GelRed for 10 min. Finally, the gel was visualized under UV irradiation using a gel image system.

2.5. Fluorescence kinetics

2.5.1. Double-stranded DNA branch migration

1 μL of 10 μM B1 and 1 μL of 10 μM B2 were added to 48 μL of buffer A (10 mM HEPES containing 20 mM $MgCl_2$, pH 7.8) and incubated for 20 min to form B1B2. A1′A2′ was formed in the same way. These two solutions were then mixed, and the fluorescence intensity was detected.

2.5.2. Cleaving activity of DNAzymes

For the 100 nM DNAzyme reaction system, 25 μL of buffer A containing 400 nM B1B2 was mixed with 25 μL of buffer A containing 400 nM A1A2 to obtain a solution containing B1A1. This solution was then added to 50 μL of 200 nM substrate chain S and the fluorescence intensity was detected. For the 4 nM DNAzyme reaction system, the B1A1 solution was diluted 25 times, and the same reaction volume was chosen.

2.5.3. DNAzyme feedback circuit

Buffer A (25 μL) containing 400 nM each of C1, C2, D1 and D2 was mixed with buffer A (25 μL) containing 400 nM B1A1. This mixture was then added to 50 μL of buffer A containing 200 nM A1''A2'', and the fluorescence intensity was detected. For the negative control, no B1A1 was added, and the total volume of the final solution remained unchanged.

2.6. Fluorescence detection of P. aeruginosa

1 μL of 10 μM each of B1, B2 and aptamer was added to 92 μL of buffer B (10 mM Tris-HCl containing 20 mM $MgCl_2$ and 100 mM NaCl, pH 7.4) for 20-min incubation. Next, 5 μL of *P. aeruginosa* solution with different concentrations was added to the above solution and incubated at 37 °C for 50 min. After *P. aeruginosa* had bound to the aptamer, the solution was centrifuged at 5000 rpm for 5 min and the supernatant containing B1B2 was collected. Next, 200 μL of buffer A containing 50 nM each of A1, A2, C1, C2, D1, and D2 and 200 μL of buffer A containing 250 nM each of H1, and H2 were mixed with the above supernatant to form a final 500 μL reaction solution. The mixture was incubated at 25 °C for 100 min. Finally, the fluorescence intensity of the reaction solution was detected.

2.7. P. aeruginosa analysis in urine samples

To evaluate the potential clinical application of the fluorescence biosensor, different concentrations of *P. aeruginosa* were added to urine samples (diluted 10 times with PBS buffer) to prepare the reaction solutions. The detection was performed under the optimum conditions and the recovery rate and relative standard deviation (RSD) were calculated.

3. Results and discussion

3.1. Principle of the biosensor for P. aeruginosa detection

The principle of the biosensor is shown in Scheme 1: First, the DNA "Y" junction structure B1B2 (B1, B2 each represents a ssDNA strand) bound to the *P. aeruginosa* aptamer to form a three-way junction (3WJ) structure. *P. aeruginosa* could bind to the aptamer specifically and release B1B2, thus triggering the double-stranded DNA branch migration with another DNA "Y" junction structure A1A2 due to the binding of the exposed double toehold regions (the red and green parts of region I and II). After a transient retention of the intermediate product, another two DNA "Y" junction structures, B1A1 and B2A2, were eventually produced. One end of B1A1 formed the active structure of a double-stranded DNAzyme (the region III), which cleaved the ribonucleotide site on C1 and C2 of a four-stranded DNA structure. Because of the

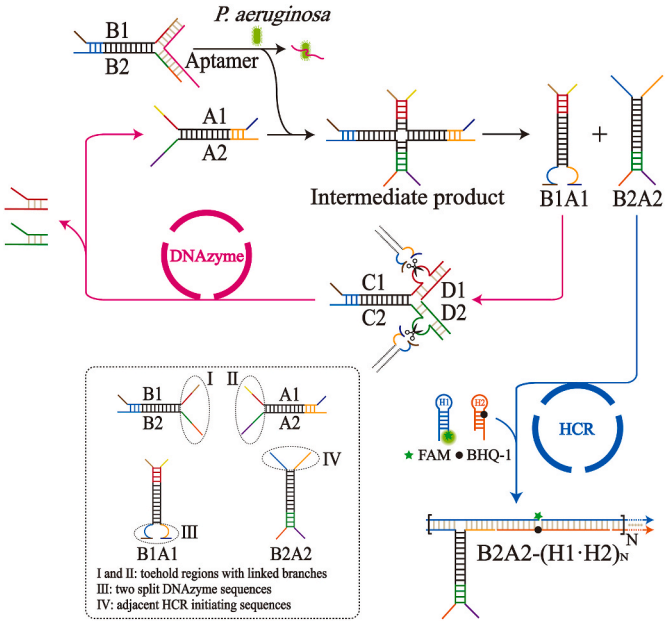

Scheme 1. Schematic of the fluorescence biosensor based on double-stranded DNA branch migration-induced HCR and DNAzyme feedback circuit for sensitive detection of *P. aeruginosa*.

binding instability, double toehold regions of C1C2 were exposed. The cleaved C1C2 again triggered the double-stranded DNA branch migration with A1A2, resulting in the accumulation of more DNA "Y" junction structures in a DNAzyme feedback circuit. In addition, B2A2 opened DNA hairpin H1 and triggered HCR due to the adjacent branches of its one end (the region IV). When long dsDNA polymers were produced, the fluorophores FAM and BHQ-1 closed to each other, which resulted in a reduced fluorescence signal. With the accumulation of B2A2, the fluorescence signal was further decreased, and thus the sensitive detection of *P. aeruginosa* was realized. When *P. aeruginosa* was absent in the solution, the double-stranded DNA branch migration could not occur because of the blocked toehold regions of B1B2 by *P. aeruginosa* aptamer, and thus only a low signal change could be detected. Obviously, based on the connection between the 3WJ structure and the HCR-DNAzyme feedback circuit through the double-stranded DNA branch migration, a sensitive sensing strategy was achieved without protein enzymes and complex signal amplification procedures.

3.2. Feasibility of the proposed biosensor

To ensure the formation of two DNA "Y" junction structures, the double-stranded DNA branch migration was initially verified. Fig. S1A showed the fundamental process of the double-stranded DNA branch migration, which is a reversible reaction to some extent. In order to produce fewer intermediate products, the toehold regions of the forward reaction (the red and green parts) and the reverse reaction (the blue and orange parts) need to be as short as possible [38]. When some short branches are linked at the ends of the DNA "Y" junction structures (Fig. S1B), the reaction kinetics has few changes. As shown in Fig. 1A, the fluorophores FAM and BHQ-1 were used to label the ends of A1A2 to form A1′A2′, respectively. The B2′ strand was introduced to make B1B2′ have one more toehold base number of the reverse reaction than that of B1B2 (5 versus 4, corresponding to the blue parts). As shown in Fig. 1B, the fluorescence signal between B1B2 and A1′A2′ was stronger than that between B1B2′ and A1′A2′ as the reaction time increased, for that the latter had more toehold base numbers in the reverse reaction, thereby making it less conducive to generating products. Moreover, we used polyacrylamide gel electrophoresis (PAGE) to characterize the formation of DNA "Y" junction structures. To distinguish the four DNA "Y" junction structures, as shown in Figs. S1C and S1D, some short branch sequences were linked at the end of B1, B2 and B2′ to form B3, B4 and B5 respectively to make the molecular weight of each DNA "Y" junction structure different (the specific DNA sequences are shown in Table S1). In Fig. 1C, as shown in lanes 5 to 8, the four DNA "Y" junction structures were distributed in different locations of lanes. As shown in lane 9 and lane 10, the products B3A1 and B4A2 occupied the majority in the reaction system, which were corresponding to lane 7 and lane 8. Meanwhile, we also used PAGE to investigate the formation of products between B3B5 and A1A2. As shown in Figs. S2 and 4 products were present simultaneously in lane 9 and lane 10, indicating that B3B5 and A1A2 did not produce B3A1 and B5A2 completely, which was consistent with its more toehold base numbers in the reverse reaction and lower fluorescence signal in Fig. 1B. These results indicated that the double-stranded DNA branch migration proceeded and successfully produced two DNA "Y" junction structures.

The aptamer is the main recognition element of the biosensor. Hence, the specific binding ability of the aptamer to *P. aeruginosa* was investigated. *S. aureus* and *A. baumannii* were used as controls. As shown in Fig. S3A-Fig. S3C, *P. aeruginosa* was able to specifically bind to the aptamer, whereas *S. aureus* and *A. baumannii* barely bound to the aptamer. In Fig. S3D, the fluorescence intensities of the supernatant of *S. aureus* and *A. baumannii* were both almost 6 times greater than that of *P. aeruginosa.* The fluorescence analysis results indicated that *P. aeruginosa* could specifically bind to aptamer. In addition, the complementary length of B1B2 and the aptamer was carried out a preliminary optimization. The lengths of the complementary region of B1B2 and the aptamer were designed to be 11, 14, 17 and 20 (the binding conditions of B1B2 and the aptamer are briefly shown in Fig. S4). The generated amounts of the two DNA "Y" junction structures were regarded as signal indicators. As shown in Fig. 2A, in the presence of

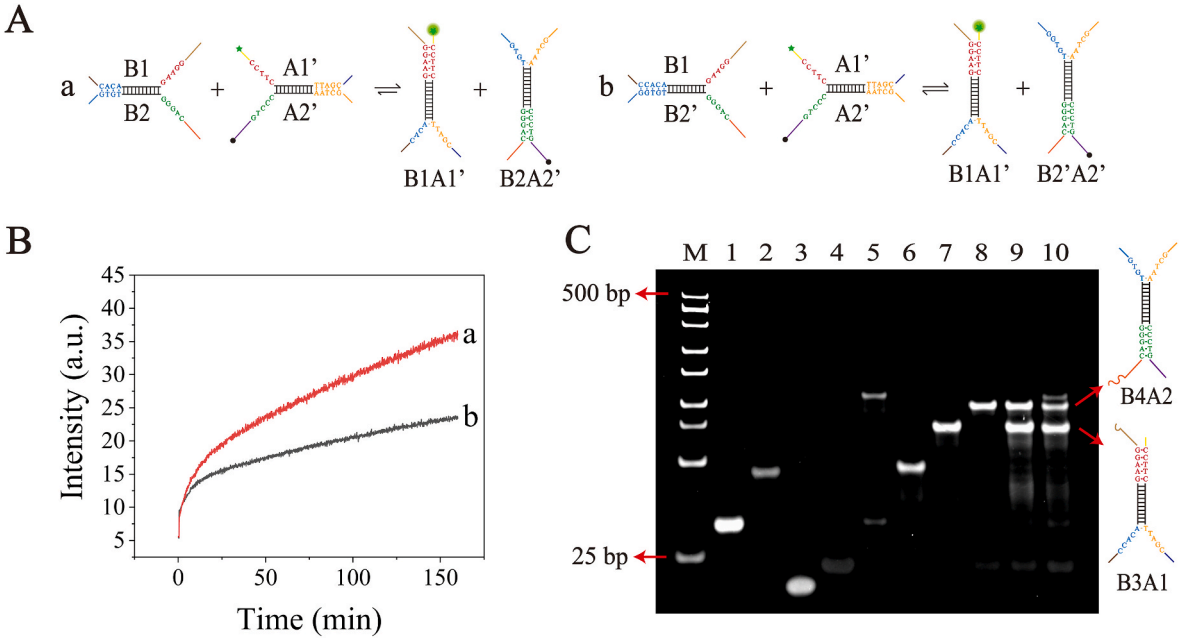

Fig. 1. (A) Double-stranded DNA branch migration between B1B2 and A1′A2′ (a) and between B1B2′ and A1′A2′ (b). B1B2′ has one more complementary base in blue parts than B1B2. (B) Time-dependent fluorescence changes of the double-stranded DNA branch migration: (a) B1B2 and A1′A2′, (b) B1B2′ and A1′A2′. (C) PAGE image of the double-stranded DNA branch migration between B3B4 and A1A2. Lane M: DNA marker (25 bp-500 bp); lane 1: B3 (750 nM); lane 2: B4 (750 nM); lane 3: A1 (750 nM); lane 4: A2 (750 nM); lane 5: B3B4 (500 nM); lane 6: A1A2 (500 nM); lane 7: B3A1 (500 nM); lane 8: B4A2 (500 nM); lane 9: B3B4 (500 nM) + A1A2 (500 nM); lane 10: B3 (500 nM) + B4 (500 nM) + A1 (500 nM) + A2 (500 nM). (For interpretation of the references to color in this figure legend, the reader is referred to the Web version of this article.)

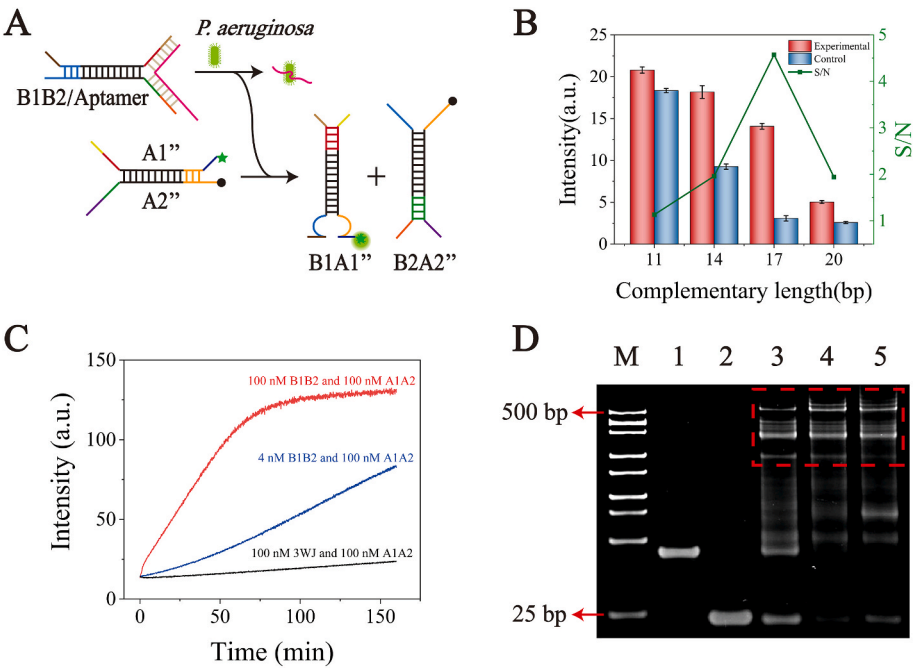

Fig. 2. (A) Principle of preliminary optimization of the length of the complementary region of B1B2/aptamer. (B) Relationship between the fluorescence intensity and the length of the complementary region of B1B2/aptamer. S/N represents the ratio of the experimental group to the control group. Error bars = SD (n = 3). (C) Verification of the cleaving activity of the double-stranded DNAzyme in the presence of 100 nM S and: 100 nM B1B2 and 100 nM A1A2 (red curve), 4 nM B1B2 and 100 nM A1A2 (blue curve), 100 nM 3WJ structure of B1B2/aptamer and 100 nM A1A2 (black curve). (D) PAGE image of B2A2-induced HCR. Lane M: DNA marker (25 bp-500 bp); lane 1: B2A2 (1 μM); lane 2: H1′ and H2′ (1 μM); lane 3: B2A2 (1 μM) + H1′ (1 μM) + H2′ (1 μM); lane 4: B2A2 (0.5 μM) + H1′ (1 μM) + H2′ (1 μM); lane 5: B2A2 (0.1 μM) + H1′ (1 μM) + H2′ (1 μM). (For interpretation of the references to color in this figure legend, the reader is referred to the Web version of this article.)

P. aeruginosa, the generated B1A1'' and B2A2'' increased the fluorescence signal. If the length of the complementary region was too short, the signal of the experimental group (with *P. aeruginosa*) and the control group (without *P. aeruginosa*) were both relatively high. In contrast, a too long complementary length would result in both having a low signal. As shown in Fig. 2B, when the length of the complementary region was 17, the signal gap between the experimental group and the control group was maximal, and the signal-to-noise ratio (S/N) also reached the maximum. Therefore, 17 complementary bases between B1B2 and the aptamer were selected in the subsequent experiments.

DNAzyme is a key part in signal amplification; hence, the cleaving activity of the double-stranded DNAzyme was next explored. The two ends of the substrate strand S were labelled with FAM and BHQ-1, respectively. As shown in Fig. S5, in the presence of 100 nM S and different concentrations of B1A1, the fluorescence signal increased to varying degrees. Similarly, in Fig. 2C, in the presence of 100 nM S and 100 nM A1A2, different concentrations of B1B2 could led to different fluorescence signals. If 100 nM 3WJ structure of B1B2/aptamer was added, the fluorescence signal was nearly horizontal because of the blocked toehold regions by the aptamer. Next we investigated the HCR process with PAGE by means of unlabelled DNA hairpins H1′ and H2′. As shown in Fig. 2D, the B2A2 band was visible in lane 1. In lane 2, DNA hairpins H1′ and H2′ formed a single clustered band, which indicated that there were no obvious signal leaks in the system in the absence of initiating probe B2A2. Once different concentrations of B2A2 were added, the bands of long dsDNA polymers emerged (lane 3, lane 4 and lane 5), accompanied by the consumption of B2A2 and the DNA hairpins H1′ and H2′. These PAGE images indicated that the HCR was

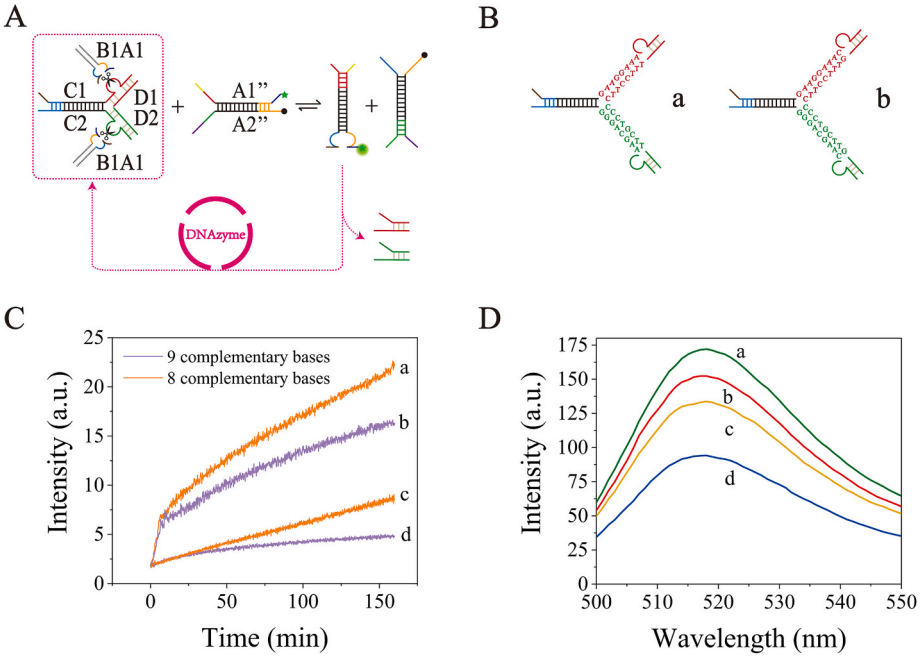

Fig. 3. (A) Principle of the B1A1-induced DNAzyme feedback circuit. (B) Two near-end binding regions with different complementary lengths between C1C2 and D1, and D2: (a) 8 complementary bases and (b) 9 complementary bases. (C) Time-dependent fluorescence changes of the B1A1-induced DNAzyme feedback circuit of two different near-end binding regions: (a) 8 complementary bases with 100 nM B1A1, (b) 9 complementary bases with 100 nM B1A1, (c) 8 complementary bases without B1A1, and (d) 9 complementary bases without B1A1. (D) Fluorescence spectra of the double-stranded DNA branch migration-induced HCR and DNAzyme feedback circuit system in the presence of *P. aeruginosa*: (a) HCR and DNAzyme feedback circuit without H2 and *P. aeruginosa*, (b) HCR and DNAzyme feedback circuit without *P. aeruginosa*, (c) HCR alone with 5×10^4 CFU mL^{-1} *P. aeruginosa*, (d) HCR and DNAzyme feedback circuit with 5×10^4 CFU mL^{-1} *P. aeruginosa*.

successfully initiated by B2A2.

Next, we explored the feasibility of the DNAzyme feedback circuit. As shown in Fig. 3A, pre-added B1A1 cleaved a specific ribonucleotide site on C1 and C2, generating unstable double chain binding regions to expose the toehold regions. The fluorescence signal subsequently rose because of the new cycle of double-stranded DNA branch migration. As shown in Fig. 3B, we designed two near-end binding regions with 8 or 9 complementary bases between C1C2 and D1 and D2, respectively. Fig. 3C shows that there was a stronger fluorescence signal regardless of whether B1A1 was added or not when the near-end binding regions contained 8 complementary bases rather than 9. Taking the reaction time of 150 min as the standard, the latter (9 complementary bases) had a higher S/N value than the former (8 complementary bases) (3.36 versus 2.54). Therefore, 9 complementary bases in the near-end binding region were selected. Next, we tested the response of the double-stranded DNA branch migration-induced HCR and DNAzyme feedback circuit system with *P. aeruginosa*. As shown in Fig. 3D, curve a exhibited a maximum peak in the absence of H2 and *P. aeruginosa*. In the presence of H2, there was a slightly decreased fluorescence peak (curve b), which indicated H1 and H2 could hardly not open to each other in the absence of *P. aeruginosa*. When *P. aeruginosa* was added, there was an obviously lower peak fluorescence signal with the HCR and the DNAzyme feedback circuit (curve d) than with the HCR alone (curve c). These results reasonably demonstrated that the proposed biosensor was applicable for the detection of *P. aeruginosa*.

3.3. Optimization of experimental conditions

To attain the optimal analysis performance of the biosensor, some of the critical experimental conditions were optimized, such as the type of working solution, the concentration ratio of B1B2/aptamer to H1/H2, the concentration ratio of B1B2/aptamer to A1/A2, the incubation time, and the temperature of the HCR and the DNAzyme feedback circuit.

Four working solutions were chosen for the detection of *P. aeruginosa* (Fig. 4A). The weakest fluorescence signal was obtained in 10 mM HEPES containing 20 mM $MgCl_2$, which was selected as the optimal working solution. Next, the concentration ratio of B1B2/aptamer to H1/H2 was optimized. The concentration of H1 and H2 was set to 100 nM. If the concentration of B1B2/aptamer was too high, there were more unblocked B1B2. By contrast, too little B1B2/aptamer would reduce the binding efficiency between *P. aeruginosa* and the aptamer. As shown in Fig. 4B, N was defined as the ratio of the initial fluorescence intensity F_0 to the eventual fluorescence intensity F. N reached the maximum value of 2.32 when c (B1B2/aptamer)/c (H1/H2) was 1:5. In addition, the concentration ratio of B1B2/aptamer to A1/A2 was also optimized. As shown in Fig. 4C, the optimal ratio of B1B2/aptamer to A1/A2 was 1:1. Finally, the incubation time and the temperature of the HCR and the DNAzyme feedback circuit were optimized. As shown in Fig. 4D, the fluorescence signal tended to plateau after the incubation time reached 100 min and was chosen as the optimal incubation time. Similarly, in Fig. 4E, we chose 25 °C as the optimal incubation temperature.

3.4. Analytical performance of the biosensor

Under the optimal experimental conditions, the analytical performance of the biosensor was evaluated by adding different concentrations of *P. aeruginosa*. As shown in Fig. 5A, the peak value of the fluorescence signal gradually reduced with increasing *P. aeruginosa* concentrations. At the same time, the difference between the original fluorescence intensity and the eventual fluorescence intensity (F_0–F) showed a linear relationship with the logarithm of *P. aeruginosa* concentrations ranging from 10^2 to 10^7 CFU mL^{-1} (Fig. 5B). The corresponding regression equation was y = 16.1984 log c −12.4942 (R^2 = 0.992). The limit of detection (LOD) was estimated to be 37 CFU mL^{-1} (S/N = 3). In addition, the analytical performance of this method in comparison with other detection strategies was summarized. As shown in Table S2, the biosensor showed a parallel or superior detection sensitivity. Notably, the biosensor offered the advantages of simplified operation and convenience with a protease-free and homogeneous reaction process. In a word, present biosensor provided a sensitive and simple detection platform for *P. aeruginosa*. Next, we investigated the specificity of the biosensor. As shown in Fig. 5C, an obvious difference (F_0–F) in signal was observed in the presence of *P. aeruginosa*, while those of the four negative control bacterial strains were all less than 30% to of the *P. aeruginosa* signal. Therefore, the biosensor has an excellent specificity for the detection of *P. aeruginosa*. Finally, the reproducibility

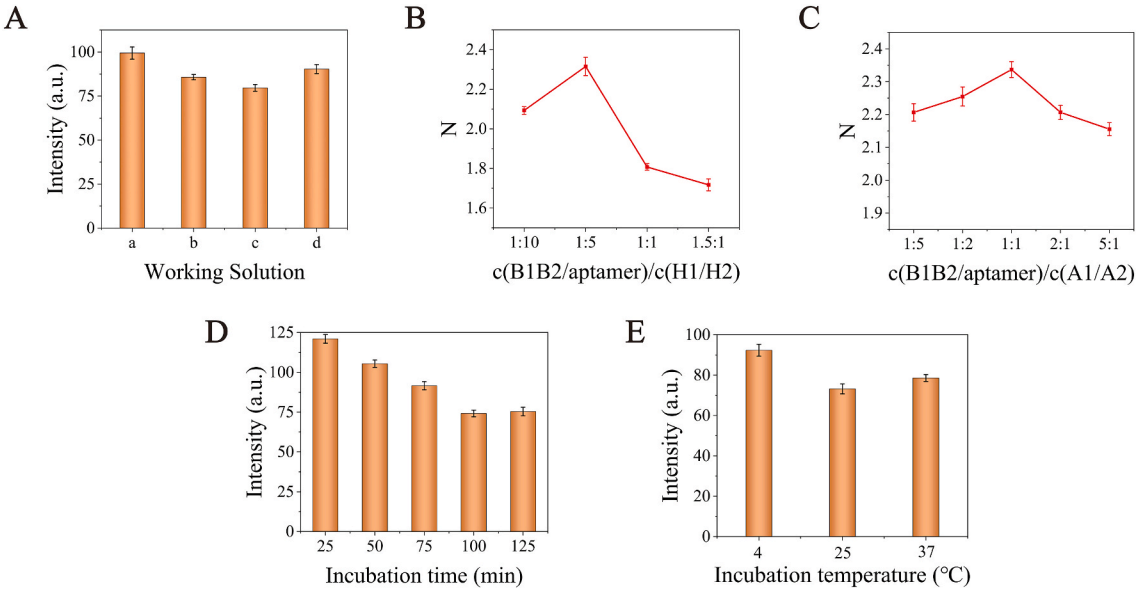

Fig. 4. Optimization of experimental conditions: (A) Type of working solution: (a) PBS, pH 7.4, (b) 10 mM Tris-HCl containing 20 mM $MgCl_2$ and 100 mM NaCl, pH 7.4, (c) 10 mM HEPES containing 20 mM $MgCl_2$, pH 7.8, (d) 10 mM HEPES containing 50 mM $MgCl_2$, pH 7.8. (B) Concentration ratio of B1B2/aptamer to H1/H2. N represents the ratio of the initial fluorescence intensity to the eventual fluorescence intensity. (C) Concentration ratio of B1B2/aptamer to A1/A2. (D) Incubation time of the HCR and the DNAzyme feedback circuit system. (E) Incubation temperature of the HCR and the DNAzyme feedback circuit system. The concentration of *P. aeruginosa* in the reaction system was kept at 10^5 CFU mL^{-1}. Error bars were derived from n = 3 experiments.

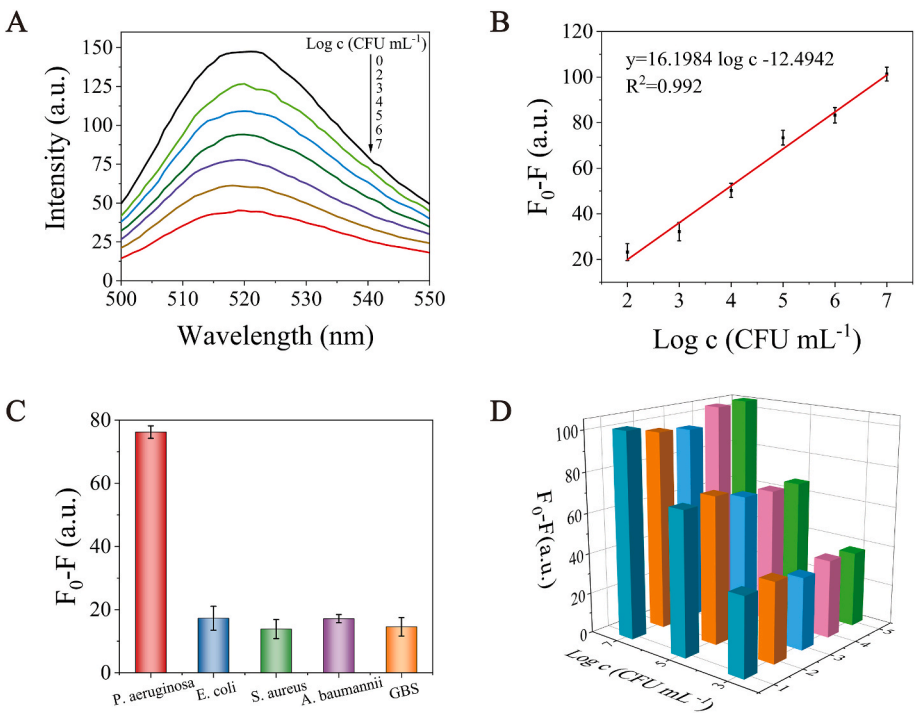

Fig. 5. Analytical performance of the fluorescence biosensor: (A) Fluorescence signals of different concentrations of *P. aeruginosa* ranging from 0 CFU mL^{-1} to 10^7 CFU mL^{-1} (from the top to the bottom of the curves). (B) Linearity of F_0–F with different concentrations of *P. aeruginosa*. F_0 represents the original fluorescence intensity. F represents the eventual fluorescence intensity (n = 3). (C) Verification of the biosensor specificity for *P. aeruginosa* compared with other bacterial strains (n = 3). (D) Reproducibility of the biosensor at *P. aeruginosa* of different concentrations for five independent experiments.

of the biosensor was evaluated. As shown in Fig. 5D, the fluorescence signals were detected five times with 10^3, 10^5 and 10^7 CFU mL^{-1} *P. aeruginosa*. The relative standard deviations (RSD) were 3.43%, 3.17% and 3.62%, respectively. These results showed that the biosensor has an excellent reproducibility and stability.

3.5. *P. aeruginosa* analysis in urine samples

To evaluate the clinical application potential of the biosensor, recovery tests were carried out in urine samples. The fresh urine samples were diluted 10 times and certain concentrations of *P. aeruginosa* were spiked. These urine samples were then detected by the constructed biosensor. All test conditions were the same as those for the standard samples, and each measurement was repeated 5 times. As shown in Table S3, the recovery rates were calculated as 96.1%–106.5% with RSDs ranging from 2.5% to 3.4%. These results indicated that the biosensor has great clinical application potential in complex biological samples.

4. Conclusions

In summary, we constructed a novel fluorescence biosensor for sensitive detection of pathogenic bacteria, represented here by *P. aeruginosa*. The biosensor has several advantages. Its protease-free and simple reaction process ensures its convenience and stability. The combined application of the HCR and the DNAzyme feedback circuit constitutes an effective signal amplification strategy. The proposed biosensor showed a wide linearity range of 10^2–10^7 CFU mL^{-1} and a low LOD of 37 CFU mL^{-1} (S/N = 3). These advantages indicate that this biosensor has good clinical application potential for the bacterial detection in biological samples. In addition, the biosensor exhibited high versatility and could detect other biological targets by replacing the specific aptamer sequence. Based on the above characteristics, this biosensor constitutes an ideal paradigm for the detection of bacterial pathogens and other biological targets. Some improvements are foreseen for this biosensor; for example, its combination with magnetic beads to realize signal separation and detection. Its incorporation into a portable point-of-care testing device should also be considered. It is believed that with the development of sensing technology, the future applications of this biosensor are promising.

CRediT authorship contribution statement

Yaxing Xie: Conceptualization, Data curation, Formal analysis, Investigation, Methodology, Writing – original draft. **Guoming Xie:** Funding acquisition, Project administration, Resources, Supervision. **Jinshan Yuan:** Data curation, Investigation, Software, Validation. **Jianhong Zhang:** Data curation, Formal analysis, Software, Visualization. **Yujun Yang:** Methodology, Resources, Validation. **Yuan Yao:** Methodology, Resources, Visualization. **You Wu:** Resources, Software. **Dan Bai:** Resources, Validation. **Kena Chen:** Software, Validation. **Baiying Li:** Software, Visualization. **Lin Song:** Software, Visualization. **Hui Chen:** Funding acquisition, Methodology, Project administration, Resources, Supervision, Writing – review & editing.

Declaration of competing interest

The authors declare that they have no known competing financial interests or personal relationships that could have appeared to influence the work reported in this paper.

Data availability

The data that has been used is confidential.

Acknowledgements

This research work was financially supported by the National Natural Science Foundation of China (No. 81972011), the Chongqing medical scientific research project (Joint project of Chongqing Health Commission and Science and Technology Bureau) (No. 2020MSXM009), and the Chongqing Technology Innovation and Application Development Special Project (cstc2019jscx-msxmX0088).

Appendix A. Supplementary data

Supplementary data to this article can be found online at https://doi.org/10.1016/j.aca.2022.340449.

References

[1] Y. Wu, G. Deng, K. Jiang, H. Wang, Z. Song, H. Han, Photothermally triggered nitric oxide nanogenerator targeting type IV pili for precise therapy of bacterial infections, Biomaterials 268 (2021), 120588.

[2] F. Jia, L. Xu, W. Yan, W. Wu, Q. Yu, X. Tian, R. Dai, X. Li, A magnetic relaxation switch aptasensor for the rapid detection of *Pseudomonas aeruginosa* using superparamagnetic nanoparticles, Microchim. Acta 184 (2017) 1539–1545.

[3] I. Jurado-Martin, M. Sainz-Mejias, S. McClean, *Pseudomonas aeruginosa*: an audacious pathogen with an adaptable Arsenal of virulence factors, Int. J. Mol. Sci. 22 (2021).

[4] X. Zheng, S. Gao, J. Wu, X. Hu, Recent advances in aptamer-based biosensors for detection of *Pseudomonas aeruginosa*, Front. Microbiol. 11 (2020), 605229.

[5] D. Li, E. Yang, Z. Luo, Q. Xie, Y. Duan, An enzyme-mediated universal fluorescent biosensor template for pathogen detection based on a three-dimensional DNA walker and catalyzed hairpin assembly, Nanoscale 13 (2021) 2492–2501.

[6] W. Bittremieux, D.L. Tabb, F. Impens, A. Staes, E. Timmerman, L. Martens, K. Laukens, Quality control in mass spectrometry-based proteomics, Mass Spectrom. Rev. 37 (2018) 697–711.

[7] Y. Xu, Y. Zhang, X. Sui, A. Zhang, X. Liu, Z. Lin, J. Chen, Highly sensitive homogeneous electrochemiluminescence biosensor for microRNA-21 based on cascaded signal amplification of target-induced hybridization chain reaction and magnetic assisted enrichment, Sensor. Actuator. B Chem. 344 (2021).

[8] M. Yang, X. Chen, L. Zhu, S. Lin, C. Li, X. Li, K. Huang, W. Xu, Aptamer-Functionalized DNA-silver nanocluster nanofilm for visual detection and elimination of bacteria, ACS Appl. Mater. Interfaces 13 (2021) 38647–38655.

[9] M. Li, J. Cheng, Z. Yuan, H. Zhou, L. Zhang, Y. Dai, Q. Shen, Q. Fan, Sensitive electrochemical detection of microRNA based on DNA walkers and hyperbranched HCR-DNAzyme cascade signal amplification strategy, Sensor. Actuator. B Chem. 345 (2021).

[10] P. Miao, Y. Tang, DNA walking and rolling nanomachine for electrochemical detection of miRNA, Small 16 (2020), e2004518.

[11] X. Chen, K. Xu, J. Li, M. Yang, X. Li, Q. Chen, C. Lu, H. Yang, Switch-conversional ratiometric fluorescence biosensor for miRNA detection, Biosens. Bioelectron. 155 (2020), 112104.

[12] Y.P. Huo, S. Liu, Z.X. Gao, B.A. Ning, Y. Wang, State-of-the-art progress of switch fluorescence biosensors based on metal-organic frameworks and nucleic acids, Mikrochim. Acta 188 (2021) 168.

[13] Z. Qiu, J. Shu, D. Tang, Bioresponsive release system for visual fluorescence detection of carcinoembryonic antigen from mesoporous silica nanocontainers mediated optical color on quantum dot-enzyme-impregnated paper, Anal. Chem. 89 (2017) 5152–5160.

[14] D. Gou, G. Xie, Y. Li, X. Zhang, H. Chen, Voltammetric immunoassay for *Mycobacterium tuberculosis* secretory protein MPT64 based on a synergistic amplification strategy using rolling circle amplification and a gold electrode modified with graphene oxide, Fe_3O_4 and Pt nanoparticles, Mikrochim. Acta 185 (2018) 436.

[15] X. Sun, Y. Wang, L. Zhang, S. Liu, M. Zhang, J. Wang, B. Ning, Y. Peng, J. He, Y. Hu, Z. Gao, A CRISPR-cas9 triggered two-step isothermal amplification method for *E. coli* O157: H7 detection based on a metal-organic framework platform, Anal. Chem. 92 (2020) 3032–3041.

[16] Z. Zhan, B. Yu, H. Li, L. Yan, Z.P. Aguilar, H. Xu, Catalytic hairpin assembly combined with graphene oxide for the detection of emetic *Bacillus cereus* in milk, J. Dairy Sci. 102 (2019) 4945–4953.

[17] C. Zhang, Z. Luo, M. Wu, W. Ning, Z. Tian, Y. Duan, Y. Li, A highly sensitive fluorescence biosensor for detection of *Staphylococcus aureus* based on HCR-mediated three-way DNA junction nicking enzyme assisted signal amplification, Analyst 146 (2021) 6528–6536.

[18] S. Bi, S. Yue, S. Zhang, Hybridization chain reaction: a versatile molecular tool for biosensing, bioimaging, and biomedicine, Chem. Soc. Rev. 46 (2017) 4281–4298.

[19] Q. Wang, M. Pan, J. Wei, X. Liu, F. Wang, Evaluation of DNA methyltransferase activity and inhibition via isothermal enzyme-free concatenated hybridization chain reaction, ACS Sens. 2 (2017) 932–939.

[20] Q. Wu, H. Wang, K. Gong, J. Shang, X. Liu, F. Wang, Construction of an autonomous nonlinear hybridization chain reaction for extracellular vesicles-associated MicroRNAs discrimination, Anal. Chem. 91 (2019) 10172–10179.

[21] J. Wei, H. Wang, X. Gong, Q. Wang, H. Wang, Y. Zhou, F. Wang, A proteinase-free DNA replication machinery for in vitro and in vivo amplified MicroRNA imaging, Nucleic Acids Res. 48 (2020) e60.

[22] Z. Yang, H. Wu, X. Yi, J. Tang, W. Yun, W. Han, X. Chen, A universal converting strategy based on target-induced DNA nanoprobe conformational change for lead (II) ion assay, Biosens. Bioelectron. 144 (2019), 111679.

[23] H. Wang, H. Wang, Q. Wu, M. Liang, X. Liu, F. Wang, DNAzyme-amplified DNA circuit for highly accurate microRNA detection and intracellular imaging, Chem. Sci. 10 (2019) 9597–9604.

[24] S. Lv, K. Zhang, Z. Lin, D. Tang, Novel photoelectrochemical immunosensor for disease-related protein assisted by hemin/G-quadruplex-based DNAzyme on gold nanoparticles to enhance cathodic photocurrent on p-$CuBi_2O_4$ semiconductor, Biosens. Bioelectron. 96 (2017) 317–323.

[25] K. Zhang, S. Lv, Z. Lin, D. Tang, CdS: Mn quantum dot-functionalized g-C_3N_4 nanohybrids as signal-generation tags for photoelectrochemical immunoassay of prostate specific antigen coupling DNAzyme concatamer with enzymatic biocatalytic precipitation, Biosens. Bioelectron. 95 (2017) 34–40.

[26] L. Yang, Q. Wu, Y. Chen, X. Liu, F. Wang, X. Zhou, Amplified MicroRNA detection and intracellular imaging based on an autonomous and catalytic assembly of DNAzyme, ACS Sens. 4 (2019) 110–117.

[27] Q. Liu, X. Sun, M. Liu, Y. Jin, B. Li, G-triplex molecular beacon–based fluorescence biosensor for sensitive detection of small molecule-protein interaction via exonuclease III–assisted recycling amplification, Sensor. Actuator. B Chem. 310 (2020).

[28] M. Liu, Q. Zhang, D. Chang, J. Gu, J.D. Brennan, Y. Li, A DNAzyme feedback amplification strategy for biosensing, Angew. Chem. Int. Ed. 56 (2017) 6142–6146.

[29] X. Liu, X. Zhou, X. Xia, H. Xiang, Catalytic hairpin assembly-based double-end DNAzyme cascade-feedback amplification for sensitive fluorescence detection of HIV-1 DNA, Anal. Chim. Acta 1096 (2020) 159–165.

[30] S.X. Chen, D.Y. Zhang, G. Seelig, Conditionally fluorescent molecular probes for detecting single base changes in double-stranded DNA, Nat. Chem. 5 (2013) 782–789.

[31] T. Wang, L. Zhou, S. Bai, Z. Zhang, J. Li, X. Jing, G. Xie, Ultraspecific electrochemical DNA biosensor by coupling spontaneous cascade DNA branch migration and dual-signaling sensing strategy, Biosens. Bioelectron. 78 (2016) 464–470.

[32] Z. Zhang, J.L. Li, J. Yao, T. Wang, D. Yin, Y. Xiang, Z. Chen, G. Xie, Energy driven cascade recognition for selective detection of nucleic acids with high discrimination factor at room temperature, Biosens. Bioelectron. 79 (2016) 488–494.

[33] T. Song, X. Guo, X. Li, S. Zhang, Label-free electrochemical detection of RNA based on "Y" junction structure and restriction endonuclease-aided target recycling strategy, J. Electroanal. Chem. 781 (2016) 251–256.

[34] Y. Ning, J. Hu, F. Lu, Aptamers used for biosensors and targeted therapy, Biomed. Pharmacother. 132 (2020), 110902.

[35] Y. Yao, G. Xie, X. Zhang, J. Yuan, Y. Hou, H. Chen, Fast detection of *E. coli* with a novel fluorescent biosensor based on a FRET system between UCNPs and GO@Fe_3O_4 in urine specimens, Anal. Methods 13 (2021) 2209–2214.

[36] D. Zhou, G. Xie, X. Cao, X. Chen, X. Zhang, H. Chen, Colorimetric determination of staphylococcal enterotoxin B via DNAzyme-guided growth of gold nanoparticles, Microchim. Acta 183 (2016) 2753–2760.

[37] H. Wang, Z. Chi, Y. Cong, Z. Wang, F. Jiang, J. Geng, P. Zhang, P. Ju, Q. Dong, C. Liu, Development of a fluorescence assay for highly sensitive detection of *Pseudomonas aeruginosa* based on an aptamer-carbon dots/graphene oxide system, RSC Adv. 8 (2018) 32454–32460.

[38] J. Li, A. Johnson-Buck, Y.R. Yang, W.M. Shih, H. Yan, N.G. Walter, Exploring the speed limit of toehold exchange with a cartwheeling DNA acrobat, Nat. Nanotechnol. 13 (2018) 723–729.